IEEE

SENSORS JOURNAL

A PUBLICATION OF THE IEEE SENSORS COUNCIL WWW.IEEE.ORG/SENSORS

This Print Collection Contains the Following Issues:

JULY 2012 VOLUME 12 NUMBER 7 ISJEAZ (ISSN 1530–437X)

For the July 2012 issue, see p. 2345 for the Table of Contents.

AUGUST 2012 VOLUME 12 NUMBER 8

For the August 2012 issue, see p. 2537 for the Table of Contents.

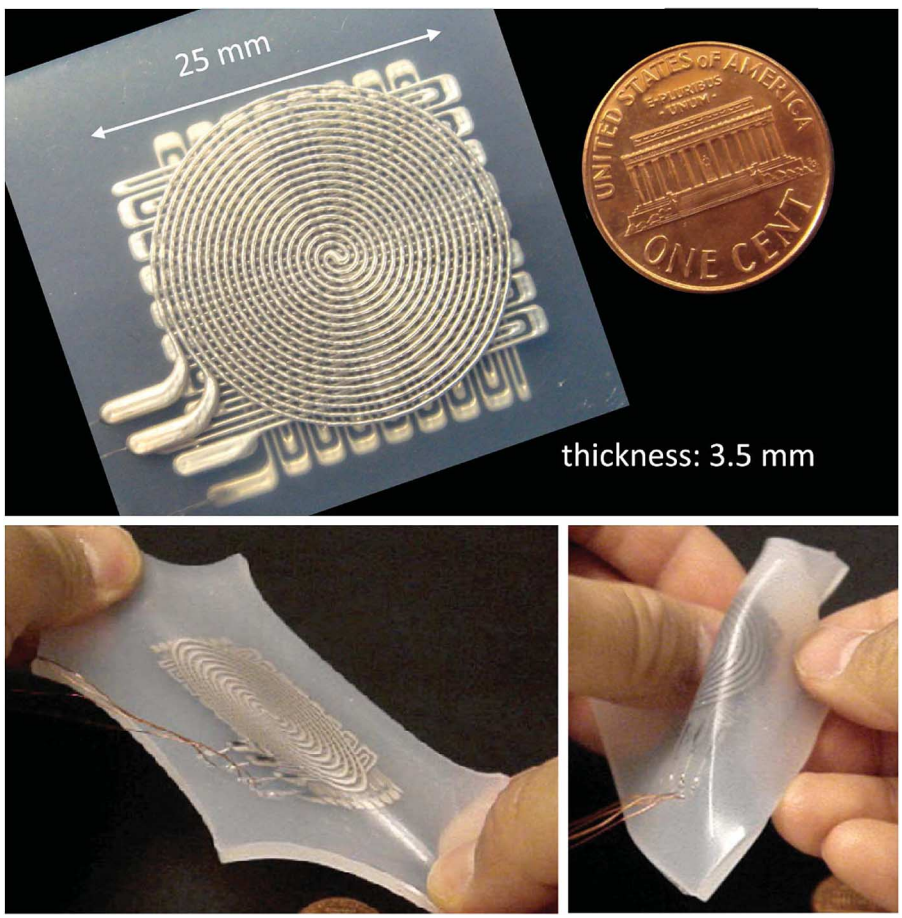

Soft artificial skin using embedded microchannels and liquid conductors (see page 2711).

Design and Fabrication of Soft Artificial Skin Using Embedded Microchannels and Liquid Conductors

Yong-Lae Park, *Member, IEEE,* Bor-Rong Chen, *Member, IEEE,* and Robert J. Wood, *Member, IEEE*

***Abstract*— We describe the design, fabrication, and calibration of a highly compliant artificial skin sensor. The sensor consists of multilayered mircochannels in an elastomer matrix filled with a conductive liquid, capable of detecting multiaxis strains and contact pressure. A novel manufacturing method comprised of layered molding and casting processes is demonstrated to fabricate the multilayered soft sensor circuit. Silicone rubber layers with channel patterns, cast with 3-D printed molds, are bonded to create embedded microchannels, and a conductive liquid is injected into the microchannels. The channel dimensions are 200 μm (width) × 300 μm (height). The size of the sensor is 25 mm × 25 mm, and the thickness is approximately 3.5 mm. The prototype is tested with a materials tester and showed linearity in strain sensing and nonlinearity in pressure sensing. The sensor signal is repeatable in both cases. The characteristic modulus of the skin prototype is approximately 63 kPa. The sensor is functional up to strains of approximately 250%.**

***Index Terms*— Artificial skin, eutectic gallium indium (EGaIn), pressure sensing, soft sensors, strain sensing.**

I. Introduction

THE DEVELOPMENT of highly deformable artificial skin (Fig. 1) with contact force (or pressure) and strain sensing capabilities [1] is a critical technology to the areas of wearable computing [2], haptic interfaces, and tactile sensing in robotics. With tactile sensing, robots are expected to work more autonomously and be more responsive to unexpected contacts by detecting contact forces during activities such as manipulation and assembly. Application areas include haptics [3], humanoid robotics [4], and medical robotics [5].

Different approaches for sensitive skin [6] have been explored. One of the most widely used methods is to detect structural deformation with embedded strain sensors in an artificial skin. Highly sensitive fiber optic strain sensors have been embedded in a plastic robotic finger for force sensing and contact localization [7], [8] and in surgical and interventional tools for force and deflection sensing [9], [10]. Embedded strain gauges have been used in a ridged rubber structure for tactile sensing [11]. Detecting capacitance change with embedded capacitive sensor [12] arrays is another approach for tactile sensing, as shown in a human-friendly robot for contact force sensing [13], [14]. Embedding conductive materials in a polymer structure is also a popular method for artificial skin such as nanowire active-matrix circuit integrated artificial skins [15], conductive polymer-based sensors [16], solid-state organic FET circuits [17], and conductive fluid embedded silicone robot fingers [18]. In spite of their flexibility, the above example sensing technologies are not truly stretchable and also cannot remain functional at large strains. For example, fiber optic sensors have upper strain limits of approximately 1–3% for silica [19] and 10% for polymers [20], and typical strain gauges cannot tolerate strains higher than 5% [21].

There have been stretchable skin-like sensors proposed using different methods. Strain sensing fabric composites for hand posture and gesture detection has been developed using an electrically conductive elastomer [22]. A stretch-

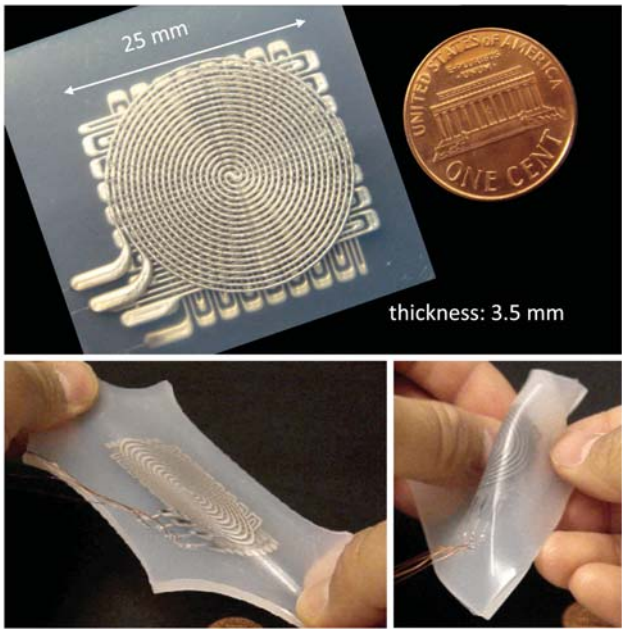

Fig. 1. Soft artificial skin prototype showing its stretchability and deformability.

Manuscript received January 16, 2012; revised April 13, 2012; accepted May 1, 2012. Date of publication May 22, 2012; date of current version June 13, 2012. This work was supported in part by the Wyss Institute for Biologically Inspired Engineering, Harvard University, and the National Science Foundation Grant CNS 0932015. This is an expanded paper from the IEEE SENSORS 2011 Conference. The associate editor coordinating the review of this paper and approving it for publication was Prof. Boris Stoeber.

Y.-L. Park is with the Wyss Institute for Biologically Inspired Engineering, Harvard University, Boston, MA 02115 USA (e-mail: ylpark@wyss.harvard.edu).

B.-R. Chen was with the School of Engineering and Applied Science, Harvard University, Cambridge, MA 02138 USA. He is now with Biosensics LLC, Cambridge, MA 02139 USA (e-mail: brchen@post.harvard.edu).

R. J. Wood is with the School of Engineering and Applied Science, Harvard University, Cambridge, MA 02138 USA, and also with the Wyss Institute for Biologically Inspired Engineering, Harvard University, Boston, MA 02115 USA (e-mail: rjwood@eecs.harvard.edu).

Color versions of one or more of the figures in this paper are available online at http://ieeexplore.ieee.org.

Digital Object Identifier 10.1109/JSEN.2012.2200790

able tactile sensor has been proposed also using polymeric composites [23]. A highly twistable tactile sensing array has been made with stretchable helical electrodes [24]. An ionic fluid has been used with an elastomer material for measuring large strains [25]. Electroconductive elastic rubber materials have been explored for measuring displacement and control of McKibben pneumatic artificial muscle actuators [26]–[28]. However, these sensors are not able to remain functional at strains over 100%.

We focus on a particular type of conductive liquid materials, i.e., eutectic gallium-indium (EGaIn) [29], which are finding increasing applications in soft wearable robots [30], flexible sensors [31] and stretchable electronics [32], [33]. EGaIn is an alloy of gallium and indium maintaining a liquid state at room temperature. Due to its high surface tension and high electrical conductance, EGaIn is an ideal conductor for a soft sensor.

In this paper, we present a highly deformable artificial robotic skin (Fig. 1) with multi-modal sensing capable of detecting strain and contact pressure simultaneously, designed and fabricated using the combined concept of hyperelastic strain and pressure sensors with embedded microchannels filled with EGaIn [34]. The prototype is able to decouple multi-axis strains as well as contact pressure at strains of more than 100%. Although there have been some efforts on developing robotic skins and structures that can detect multiple types of stimuli [35], [36], highly deformable and stretchable materials have not been fully explored for multi-modal sensing.

To the best of our knowledge, this is the first approach to make an artificial skin that provides multi-modal sensing capability with a highly soft and stretchable material using an embedded liquid conductor. The rest of the paper is organized as follows. Section II discusses the design concept of the artificial skin. Section III describes the fabrication process using a new variation of a rapid prototyping process. Section IV presents the characterization procedures and results. Section V describes the integrated system for real-time multi-modal sensing. We conclude with a discussion of future work, which includes improvement on the sensor linearity for contact pressure sensing.

II. Design

The sensing principles of our artificial skin are simple. When the microchannels filled with EGaIn are deformed by either pressing or stretching, the electrical resistance of the microchannels increases due to their reduced cross-sectional areas, increased channel lengths, or both.

A. Strain Sensing

The design concept of strain sensing is adapted from a rubber strain sensor that contains mercury in a rubber tube [37], [38]. When the material experiences strain in the axial direction of the channels, the overall channel length increases and the cross-sectional areas of the channels decrease, as shown in Fig. 2(b), which causes an increase in the overall resistance of the channel. Since the microchannels are filled with EGaIn, the strain sensor is highly flexible and stretchable. The theoretical

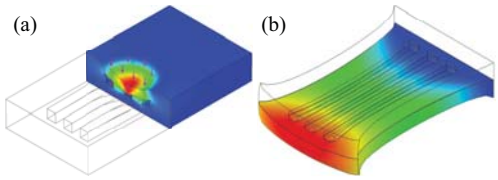

Fig. 2. Hyperelastic sensor design concepts. (a) Pressure sensing. (b) Strain sensing.

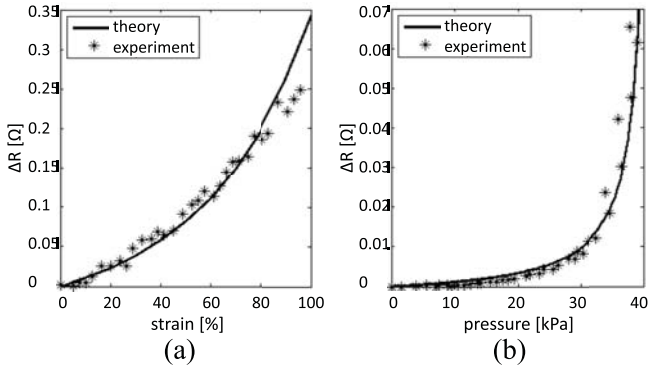

Fig. 3. Comparison between theoretical and experimental results using single microchannels. (a) Strain sensing ($w = 0.6$ mm, $h = 0.5$ mm, $L = 50$ mm, and $\rho = 29.4 \times 10^{-8} \Omega$ m^{-1}). (b) Pressure sensing ($w = 2$ mm, $h = 1$ mm, and $E = 125$ kPa).

relationship between the resistance change (ΔR) and strain (ϵ) can be easily found as follows:

$$\Delta R = R - R_0 = \rho \frac{L + \Delta L}{(w + \Delta w)(h + \Delta h)} - \rho \frac{L}{wh} \qquad (1)$$

where R and R_0 are the resistances of the microchannel when stretched by ΔL and not stretched, respectively, ρ is the electrical resistivity of EGaIn, L is the length of the microchannel, and w and h are the width and height of the cross-section of the microchannel, respectively.

By replacing Δw and Δh with $-\nu\epsilon w$ and $-\nu\epsilon h$, respectively, and since $\epsilon = \Delta L / L$

$$\Delta R = \frac{\rho L}{wh} \left\{ \frac{(1 + 2\nu)\epsilon - \nu^2 \epsilon^2}{(1 - \nu\epsilon)^2} \right\} \qquad (2)$$

where ν is the Poisson's ratio of the elastomer material.

For an elastomer material ($\nu = 0.5$), we can further simplify the above equation to

$$\Delta R = \frac{\rho \epsilon L (8 - \epsilon)}{wh(2 - \epsilon)^2}. \qquad (3)$$

Fig. 3(a) shows comparison between theoretical and experimental result of strain sensing using a single microchannel.

B. Pressure Sensing

Pressing the surface of the elastomer skin decreases the cross-sectional area of the microchannels and increases their electrical resistance, as shown in Fig. 2(a). The relationship between the resistance change (ΔR) and contact pressure (p) can be theoretically modeled [34] using linear elastic fracture mechanics (LEFM) [39], [40]. Under the assumption that the

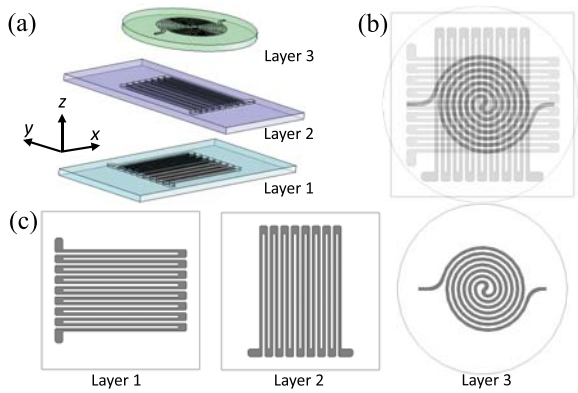

Fig. 4. Design of the three sensor layers with embedded microchannels. (a) Exploded view. (b) Assembled view. (c) Each sensor layer design (Layer 1: x-axis strain sensing, Layer 2: y-axis strain sensing, and Layer 3: z-axis pressure sensing).

cross-section of the microchannel is square, the resistance change is expressed as

$$\Delta R = \frac{\rho L}{wh}\left\{\frac{1}{1-2(1-\nu^2)wp/Eh}-1\right\} \tag{4}$$

where and E is the elastic modulus of the elastomer material. Comparison between theoretical and experimental results of pressure sensing is shown in Fig. 3(b).

C. Skin Design

The overall design includes three soft sensor layers made of silicone rubber (Fig. 4) that is highly stretchable and compressible (modulus: 69 kPa, shore hardness: 00–30). Layers 1 and 2 have straight-line microchannels with a strain gauge pattern that results in directional sensitivity in axial directions as well as surface pressure sensitivity, and Layer 3 has circular patterned microchannels that are sensitive to surface pressure but are not directionally sensitive to strains along any axis. Layer 2 is placed on top of Layer 1 with a 90° rotation for detecting strain along a perpendicular axis. Using the combination of the signals from the three sensors, the device is able to detect and distinguish three different stimuli: x-axis strain, y-axis strain, and z-axis pressure Fig. 4(a).

The details of the complete prototype are shown in Fig. 5. All three sensor layers are connected through interconnects [p_2 and p_3 in Fig. 5(b)] between layers, making one circuit that is electrically equivalent to three variable resistors connected in series.

III. Fabrication

The sensor prototype was fabricated using a layered molding and casting process, as shown in Fig. 6. The process can be divided into three steps, casting, bonding, and EGaIn injection.

The base material is silicone rubber,[1] which is chosen for its combination of high stretchability (elongation at failure: 900%) and ease of casting at room temperature. A relatively low mixed viscosity (3000 cps) is an additional consideration in order to successfully reproduce the features of the mold.

[1]EcoFlex0030, Smooth-On, Inc., Easton, PA 18042, USA.

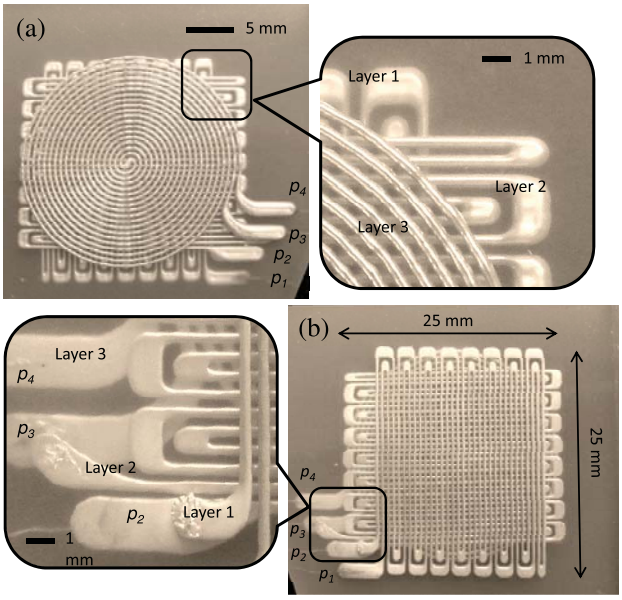

Fig. 5. Actual prototype of the multilayered soft artificial skin sensor with embedded EGaIn microchannels. (a) Front side of the prototype showing the pressure sensor (Layer 3) on top and its magnified view showing the multilayered structure; p_1, p_2, p_3, and p_4 are the EGaIn reservoirs for wire connections. (b) Back side of the prototype showing the bottom strain sensor (Layer 1) on top and its magnified view showing the interconnects, p_2 and p_3, for connecting Layers 1 to 2 and Layers 2 to 3, respectively.

The first step is to cast separate sensor layers Fig. 6(a) and (b). Plastic molds are prepared using a 3-D printer,[2] and liquid silicone is poured into the molds. The liquid silicone is cured at room temperature for more than three hours. Elevated temperature (approximately 60 °C) may accelerate the curing process of polymer materials.

The second step is to bond layers to make a single sensor structure Fig. 6(c)–(f). The cured layers are bonded by spin-coating the same liquid silicone between the layers. A small piece of plastic is inserted in the interconnect hole before spin-coating to prevent the liquid silicone blocking the hole and removed before bonding layers. The actual bonding process does not require any additional heat or pressure, although partial curing at 60 °C for one minute of the spin-coated silicone helps preventing the silicone from flowing into microchannels. A single sensor structure is made by repeating this spin-coating and bonding process. Also, alignment posts in the molds facilitate aligning the interconnects between layers. Fig. 7 shows how each layer is bonded to the previous layer with the alignment, described in Fig. 6(c)–(e). In each bonding step, alignment is important to ensure the channel connection between layers through the interconnects. The diameter of the interconnect hole is 1 mm.

In the final step, EGaIn[3] is injected into the microchannels using two syringes. One syringe injects EGaIn, and the other syringe extracts air captured in the microchannels Fig. 6(g). When connected, the three sensors form one continuous channel, thus only a single filling step is required. Finally, wire connections are made by inserting electrodes Fig. 6(h).

[2]Connex500, Objet Geometries Ltd., Billerica, MA 01821, USA.

[3]Gallium-Indium eutectic, 495425, Sigma-Aldrich, St. Louis, MO 63103.

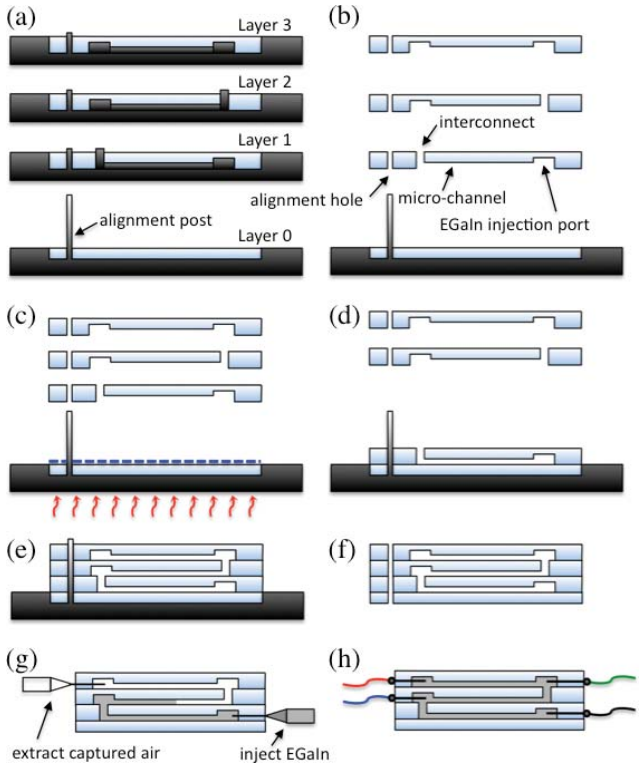

Fig. 6. Fabrication process. (a) Prepare molds and pour liquid silicone. (b) Remove molds when the silicone cures. (c) Spin-coat Layer 0 (2000 rpm for 50 s.) and partially cure (60 °C for 1 min.). (d) Bond Layers 1 to 0. (e) Bond Layers 2 and 3 by repeating spin-coating and partial curing. (f) Remove mold of Layer 0. (g) Inject EGaIn using syringes. (h) Connect wire by inserting electrodes.

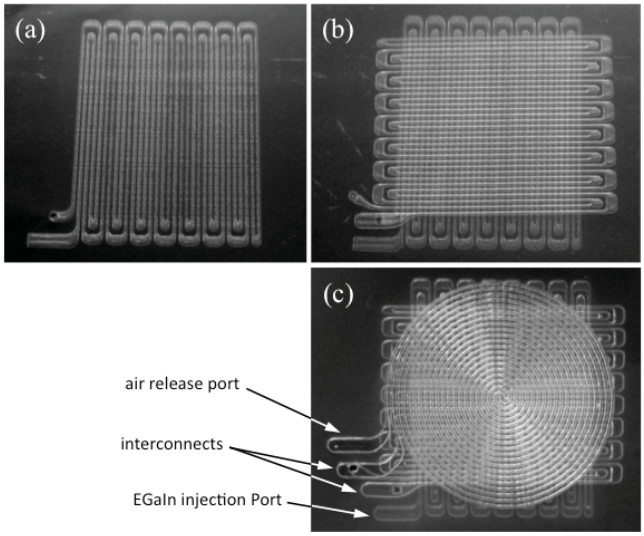

Fig. 7. Photos of microchannel embedded silicone layers showing the layer bonding steps. (a) Layer 1. (b) Layers 1 and 2. (c) Layers 1, 2, and 3.

The punctures made by the wire connections can be sealed using the same silicone material. The thickness of each layer is approximately 0.75 mm making the overall thickness of the complete skin prototype with appropriate sealing approximately 3.5 mm. Fig. 8 shows how the multiple sensor layers are filled with EGaIn with a single injection. The entire length of the microchannels in our prototype is approximately

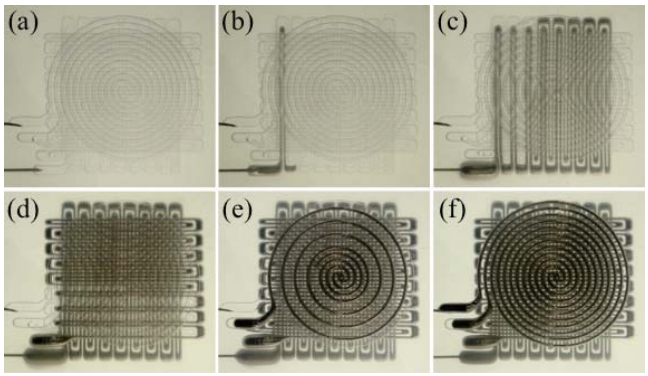

Fig. 8. Snapshots of the EGaIn injection process. (a) Empty microchannels before injection. (b) Start of injection. (c) Layer 1 injection. (d) Layer 2 injection. (e) Layer 3 injection. (d) Finished prototype.

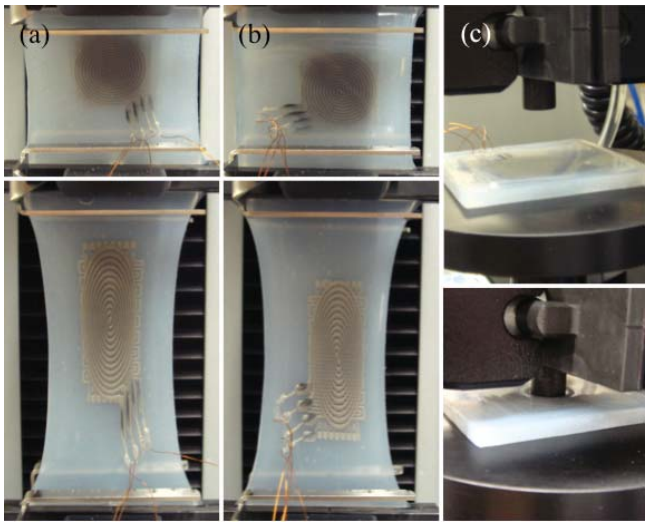

Fig. 9. Experiment setups for sensor characterization. (a) x-axis strain test. (b) y-axis strain test. (c) z-axis pressure test.

2.25 m, and the EGaIn injection process takes approximately one minute.

A complete prototype of the artificial skin is shown in Fig. 5. The channel dimension is 200 μm (width) $\times$ 300 μm (height) for all three layers. The overall size of the artificial skin is 25 mm $\times$ 25 mm.

IV. Characterization

Fig. 9 shows the experimental setups for three different calibration tests: x and y-axis strain tests and z-axis surface pressure test. The nominal resistance of each sensor layer at rest is 2.6 Ω, 2.5 Ω, and 3.1 Ω for Sensors 1, 2, and 3, respectively. A commercial material tester[4] was used for all the characterization experiments.

A. Strain Response

The strain response of the skin prototype was calibrated by applying axial strains in two perpendicular directions: the x and y axes. The prototype was gradually stretched multiple times with various rates (1 mm/sec, 2 mm/sec, 4 mm/sec, and

[4]Instron 5544A, Instron, Norwood, MA 02062, USA.

8 mm/sec) up to 100% in the x and y axes, separately, as shown in Fig. 9(a) and (b), and the resistance changes of the three sensors were measured. The calibration results for both axes, in Fig. 10(a) and (b), showed linearity in strain sensing, and the sensor signal was repeatable. With linear fitting of the sensor signals in Fig. 10(a) and (b), the gauge factor (G) of the strain sensor can be found as follows:

$$\frac{\Delta R}{R} = G\epsilon + \alpha\theta \tag{5}$$

where ΔR is the resistance change, R is the original resistance at rest, ϵ is the applied strain, α is the temperature coefficient, and θ is the temperature change. Since the temperature change during the experiments was negligible, the experimental gauge factors are 3.6 for x-axis strain sensing [from Sensor 1 in Fig. 10(a)] and 3.7 for y-axis strain sensing [from Sensor 2 in Fig. 10(b)].

Since the sensor signals for strain sensing are approximately linear, simultaneous strain measurement of both axes can be achieved by determining a calibration matrix [10], [41], [42], $\mathbf{C}$, when $\mathbf{y}$ and $\mathbf{s}$ are measured reference and sensor signals, respectively

$$\mathbf{y} = \mathbf{s} \cdot \mathbf{C} \tag{6}$$

where $\mathbf{y} = \begin{bmatrix} l_x & l_y \end{bmatrix}$ and $\mathbf{s} = \begin{bmatrix} s_1 & s_2 \end{bmatrix}$. l_x and l_y are the length changes of the skin in x and y axes, respectively, and s_1 and s_2 are the resistance changes of Sensors 1 and 2, respectively.

Using the Moore–Penrose pseudoinverse, the calibration matrix is

$$\mathbf{C} = \left[\mathbf{s^T s}\right]^{-1} \mathbf{s^T} \cdot \mathbf{y}. \tag{7}$$

Then, the error in measuring the length change of the skin is

$$\mathbf{e} = \mathbf{s} \cdot \mathbf{C} - \mathbf{y}. \tag{8}$$

The calibration matrix for this sensor is

$$\mathbf{C} = \begin{pmatrix} 5.54 & 0.81 \\ 0.98 & 5.76 \end{pmatrix}.$$

Using the calibration matrix, we can estimate the length changes of the skin in both x and y axes simultaneously from the sensor signals. Our experiments yielded RMS displacement errors of 1.6 mm in the x-axis and 1.8 mm in the y-axis.

B. Pressure Response

z-axis pressure response was also characterized by applying compression multiple times at the center of the top surface of the skin with a flat circular surface (diameter: 10 mm) up to 50 kPa, as shown in Fig. 9(c), with various compression rates (1 mm/sec, 1.5 mm/sec, and 2 mm/sec). Fig. 10(c) shows the experimental pressure response. The top layer (Sensor 3) showed the highest sensitivity. Considering the noise level of the sensor signals, the minimum detectable pressure is approximately 15 kPa. The pressure response is nonlinear as expected from Equation (4). While the sensitivity in a high pressure range (over 40 kPa) slightly decreased with an increased compression rate, the repeatability of sensor signal was improved, as shown in the inset of Fig. 10(c).

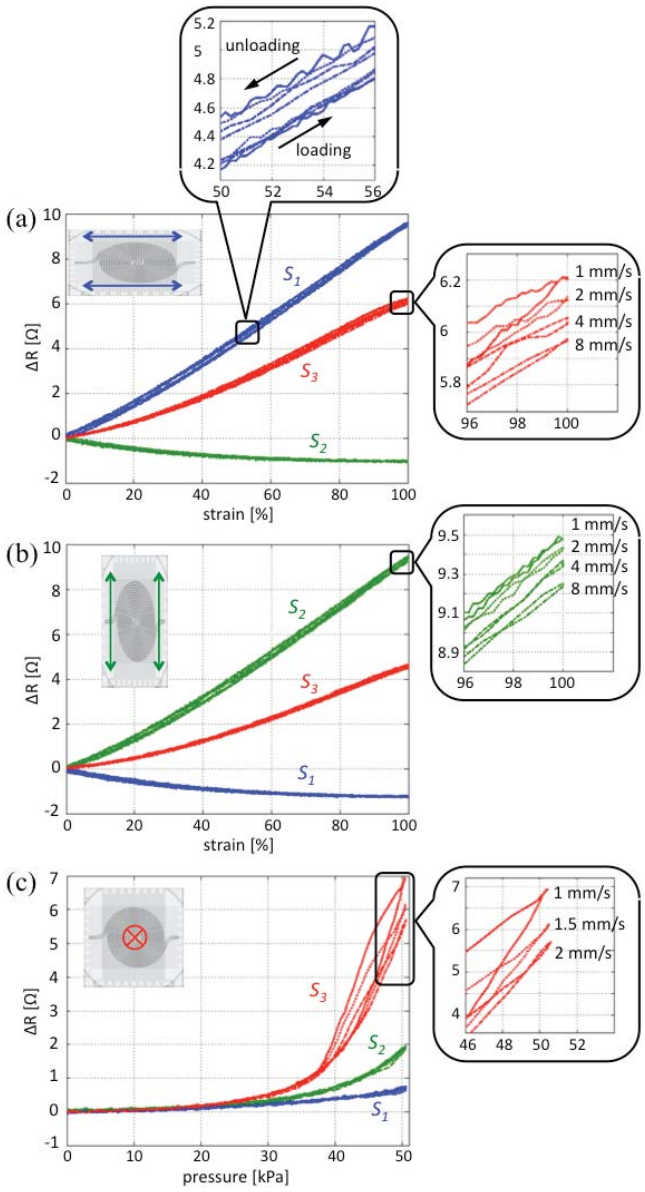

Fig. 10. Calibration results: (a) x-axis strain. (b) y-axis strain. (c) z-axis pressure.

C. Hysteresis Analysis

Polymer-based sensors generally have a certain amount of hysteresis. All the calibration test results contain loading and unloading loops, as shown in the first inset of Fig. 10(a), to characterize the hysteresis levels. While the prototype displays negligible hysteresis in strain sensing, it shows noticeable hysteresis in pressure sensing especially in a high pressure range over 40 kPa. The hysteresis level also changed with varied compression rates. As the compression rate increases from 1 mm/sec to 2 mm/sec, the hysteresis level decreases, as shown in Fig. 10(c).

D. Stimulus Differentiation

Since the signals from the three sensor layers displayed different responses in each experiment, the prototype is able not only to measure the magnitude of the stimulus but also

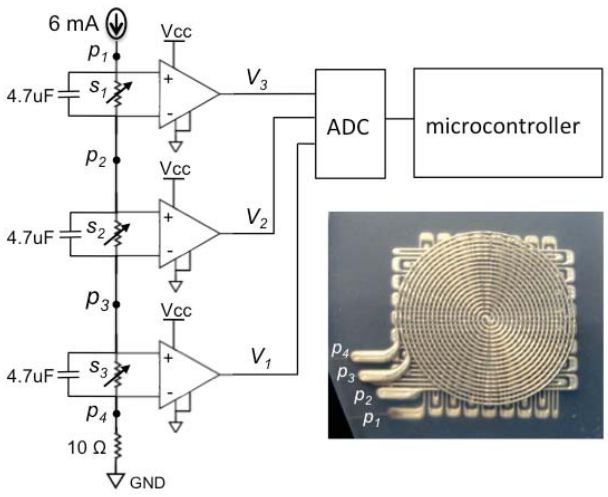

Fig. 11. Circuit diagram to read the sensor signals. p_1, p_2, p_3, and p_4 are the wire connection ports.

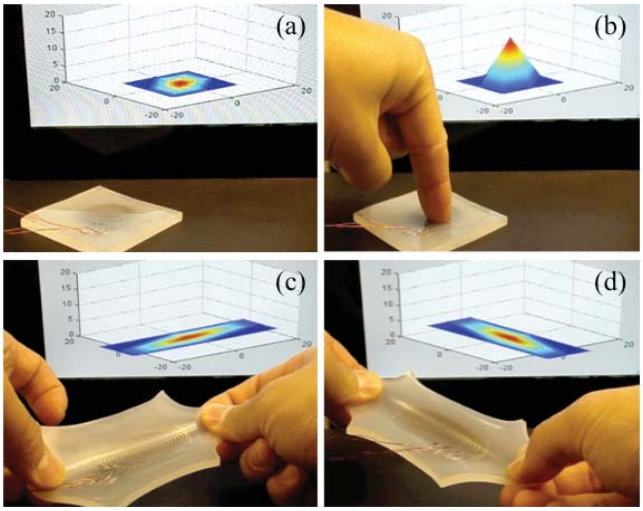

Fig. 12. Prototype in action. (a) No stimulus. (b) Contact pressure sensing. (c) x-axis strain sensing. (d) y-axis strain sensing. (The color gradient represents the center of the sensing area. It is not directly related to the sensor signal.)

to identify the type of stimulus. One example strategy is comparing the signs of the three sensor signals such as

1) If $V_1 > 0$ and $V_2 < 0$, the stimulus is x-axis strain,
2) If $V_1 < 0$ and $V_2 > 0$, the stimulus is y-axis strain,
3) If all three sensor signals are positive, the stimulus is z-axis strain.

Once the type of the stimulus is identified, we can estimate the magnitude of the stimulus from the calibration results.

The limitation of this strategy is that it is not capable of decoupling more than one type of stimuli at the same time. For example, if the surface of the skin is compressed while the skin is stretched, the system is not able to decouple the two stimuli, pressure and strain. However, it is possible to include pressure response in the calibration matrix for decoupling pressure from strain if the pressure response was made more linear.

V. System Integration

Fig. 11 shows the circuit diagram to read signals from the three sensor layers. A constant current source generates current that flows through the three sensors in series, creating voltage drops at each sensor layer. The voltage difference across each sensor is amplified by an instrumentation amplifier. The amplified signals are then connected to three analog-to-digital conversion ports of a micro-controller to measure the resistance changes.

The sensor can easily be interfaced with a computer and become a novel input device. For example, using the calibration described in the previous section, we show that a real-time pressure and strain monitoring system can be realized. Fig. 12 shows snapshots of the prototype in action. In this prototype, the sensor signal was sampled and processed using an 8-bit microcontroller[5] at 50 Hz. An Arduino was chosen as the embedded system software platform due to its user-friendly development environment. The Arduino program performed data acquisition and transmission to a laptop computer over a USB serial interface. The microcontroller transfers the resistance changes of all three sensor layers to the laptop computer in real time at 50 Hz. The resistance changes were then read by a MATLAB[6] program that included information on the calibration parameters for estimating the strain and pressure changes. Finally, the MATLAB program generated a virtual model of the skin that changes shape based on the sensor readings in real time. One can imagine such a setup to be adapted to implement novel touch− and stretch-based user interface for various applications such as computer games.

VI. Discussion

The main contribution of this work is the design of a multi-layered soft artificial skin and the development of a novel fabrication method. The current design provides multi-modal sensing capability requiring no additional sensors. There will be various applications of this technology. Immediate applications may include artificial skins for humanoid robots [4], robotic prosthetics [43], soft wearable robots [30], [44], human-friendly robots for human-robot interactions (HRI) [45], and human-computer interface (HCI). Furthermore, due to the highly flexible and stretchable properties and thin form-factor, this soft skin technology can be directly integrated with any type of soft actuator.

Although the smallest channel size is 200 μm, limited by the resolution of the 3-D printer used for making molds, this could be further reduced by implementing different manufacturing methods such as micromachined molds [46] and soft lithography [47], [48]. More compact and sensitive skins could be achieved by reducing the channel size.

While the current design showed linear and repeatable responses in strain sensing, it showed a nonlinear response and a high hysteresis level in pressure sensing, as already modeled and experimentaly shown in [34]. The nonlinearity in pressure sensing is due to the nonlinear areal reduction rate of the rectangular microchannels when contact pressure is applied. Improvement on the linearity in pressure sensing is currently

[5]Atmega328P, Atmel, San Jose, CA 95131, USA.

[6]The MathWorks Inc., Natick, MA 01760, USA.

being investigated by changing the channel geometry. The hysteresis could be also reduced by increasing the aspect ratio of the microchannels. Improving linearity and repeatability in pressure sensing is an active ongoing research area.

During fabrication, EGaIn injection in the multi-layered structure through the inter-layer interconnects makes the fabrication process simple. However, it will not be practical for filling an extremely long channel and/or a higher number of channels. A new manufacturing method that does not require the EGaIn injection step is another ongoing effort to enable faster and higher volume production.

The polymer microchannel structure showed structural robustness enough to remain functional against more than 100 strain tests. However, the first failure was observed at the wire connection site that is a mechanical interface between soft and rigid materials. When stretched excessively or repeatedly, the elastomer started to delaminate from the rigid metal electrodes. The sensor structure started to fail at strain of approximately 250%. One alternative to the current wire connection method is using a flexible circuit interface, made from polyimide/copper laminate, directly bonded to the end of the microchannel [49].

VII. Conclusion

A highly elastic artificial skin was developed using an embedded liquid conductor. Three hyper-elastic silicone rubber layers with embedded microchannels were stacked and bonded. The three layers contain different channel patterns for different types of sensing such as multi-axial strain and contact pressure. A novel manufacturing method with layered molding and casting techniques was developed to build a multi-layered soft sensor circuit.

The artificial skin prototype has channel dimensions of 200 μm (width) $\times$ 300 μm (height) for all three layers. The overall size of the artificial skin is 25 mm $\times$ 25 mm and the thickness of the skin is approximately 3.5 mm. The characteristic modulus of the skin found during the characterization experiments is approximately 63 kPa. The sensor is functional up to the strain of approximately 250%.

For strain sensing, the calibration results showed linear and repeatable sensor signal. The gauge factors of the skin prototype are 3.93 and 3.81 in x and y axes, respectively, and the minimum detectable displacements are 1.5 mm in x-axis and 1.6 mm in y-axis. For pressure sensing, the prototype showed repeatable but not linear sensor signals. The hysteresis level was high in a high pressure range (over 25 kPa). The sensor signal was repeatable in both cases.

References

[1] Y.-L. Park, B. Chen, and R. J. Wood, "Soft artificial skin with multimodal sensing capability using embedded liquid conductors," in *Proc. IEEE Sensors Conf.*, Limerick, Ireland, Oct. 2011, pp. 1–3.

[2] D. Marculescu, R. Marculescu, N. H. Zamora, P. Stanley-Marbell, P. K. Khosla, S. Park, S. Jayaraman, S. Jung, C. Lauterbach, W. Weber, T. Kirstein, D. Cottet, J. Grzyb, G. Tröster, M. Jones, T. Martin, and Z. Nakad, "Electronic textile: A platform for pervasive computing," *Proc. IEEE*, vol. 91, no. 12, pp. 1995–2018, Dec. 2003.

[3] A. Okamura and M. R. Cutkosky, "Feature detection for haptic exploration with robotic fingers," *Int. J. Robot. Res.*, vol. 20, no. 12, pp. 925–938, 2001.

[4] R. Tajima, S. Kagami, M. Inaba, and H. Inoue, "Development of soft and distributed tactile sensors and the application to a humanoid robot," *Adv. Robot.*, vol. 16, no. 4, pp. 381–397, 2002.

[5] P. Puangmali, K. Althoefer, L. D. Seneviratne, D. Murphy, and P. Dasgupta, "State-of-the-art in force and tactile sensing for minimally invasive surgery," *IEEE Sensors J.*, vol. 8, no. 4, pp. 371–381, Apr. 2008.

[6] V. J. Lumelsky, M. S. Shur, and S. Wagner, "Sensitive skin," *IEEE Sensors J.*, vol. 1, no. 1, pp. 41–51, Jun. 2001.

[7] Y.-L. Park, K. Chau, R. J. Black, and M. R. Cutkosky, "Force sensing robot fingers using embedded fiber Bragg grating sensors and shape deposition manufacturing," in *Proc. IEEE Int. Conf. Robot. Autom.*, Rome, Italy, May 2007, pp. 1510–1516.

[8] Y.-L. Park, S. C. Ryu, R. J. Black, K. Chau, B. Moslehi, and M. R. Cutkosky, "Exoskeletal force-sensing end-effectors with embedded optical fiber-Bragg-grating sensors," *IEEE Trans. Robot.*, vol. 25, no. 6, pp. 1319–1331, Dec. 2009.

[9] I. Iordachita, Z. Sun, M. Balicki, J. U. Kang, S. J. Phee, J. Handa, P. Gehlbach, and R. Tayolor, "A sub-millimetric, 0.25 mN resolution fully integrated fiber-optic force-sensing tool for retinal microsurgery," *Int. J. Comput. Assist. Radiol. Surg.*, vol. 4, no. 4, pp. 383–390, 2009.

[10] Y.-L. Park, S. Elayaperumal, B. Daniel, S. C. Ryu, M. Shin, J. Savall, R. J. Black, B. Moslehi, and M. R. Cutkosky, "Real-time estimation of 3-D needle shape and deflection for MRI-guided interventions," *IEEE/ASME Trans. Mechatron.*, vol. 15, no. 6, pp. 906–915, Dec. 2010.

[11] D. Yamada, T. Maeno, and Y. Yamada, "Artificial finger skin having ridges and distributed tactile sensors used for grasp force control," *J. Robot. Mechatron.*, vol. 14, no. 2, pp. 140–146, 2002.

[12] N. Kirchner, D. Hordern, D. Liu, and G. Dissanayake, "Capacitive sensor for object ranging and material type identification," *Sensors Actuat., A*, vol. 148, no. 1, pp. 96–104, 2008.

[13] J. Ulmen and M. Cutkosky, "A robust, low-cost and low-noise artificial skin for human-friendly robots," in *Proc. IEEE Int. Conf. Robot. Autom.*, Anchorage, AK, May 2010, pp. 4836–4841.

[14] S. Phan, Z. F. Quek, P. Shah, D. Shin, Z. Ahmed, O. Khatib, and M. Cutkosky, "Capacitive skin sensors for robot impact monitoring," in *Proc. IEEE/RSJ Int. Conf. Intell. Robot. Syst.*, San Francisco, CA, Sep. 2011, pp. 2992–2997.

[15] K. Takei, T. Takahashi, J. C. Ho, H. Ko, A. G. Gillies, P. W. Leu, R. S. Fearing, and A. Javey, "Nanowire active-matrix circuitry for low-voltage macroscale artificial skin," *Nature Mater.*, vol. 9, no. 10, pp. 821–826, 2010.

[16] S. Nambiar and J. T. Yeow, "Conductive polymer-based sensors for biomedical applications," *Biosensors Bioelectron.*, vol. 26, no. 5, pp. 1825–1832, 2010.

[17] H. Kawaguchi, T. Someya, T. Sekitani, and T. Sakurai, "Cut-and-paste customization of organic FET integrated circuit and its application or electronic artificial skin," *IEEE J. Solid-State Circuits*, vol. 40, no. 1, pp. 177–185, Jan. 2005.

[18] N. Wettels, D. Popovic, V. J. Santos, R. S. Johansson, and G. E. Loeb, "Biomimetic tactile sensor array," *Adv. Robot.*, vol. 22, no. 8, pp. 829–849, 2008.

[19] M. C. J. Large, J. Moran, and L. Ye, "The role of viscoelastic properties in strain testing using microstructured polymer optical fibres (mPOF)," *Meas. Sci. Technol.*, vol. 20, no. 3, p. 034014, 2009.

[20] K. Peters, "Polymer optical fiber sensors - a review," *Smart Mater. Struct.*, vol. 20, no. 1, pp. 013002-1–013002-17, 2011.

[21] M. Pyo, C. C. Bohn, E. Smela, J. R. Reynolds, and A. B. Brennan, "Direct strain measurement of polypyrrole actuators controlled by the polymer/gold interface," *Chem. Mater.*, vol. 15, no. 4, pp. 916–922, 2003.

[22] F. Lorussi, E. P. Scilingo, M. Tesconi, A. Tognetti, and D. De Rossi, "Strain sensing fabric for hand posture and gesture monitoring," *IEEE Trans. Inf. Technol. Biomed.*, vol. 9, no. 3, pp. 372–381, Sep. 2005.

[23] L. Ventrelli, L. Beccai, V. Mattoli, A. Menciassi, and P. Dario, "Development of a stretchable skin-like tactile sensor based on polymer composites," in *Proc. IEEE Int. Conf. Robot. Biomimet.*, Guilin, China, Dec. 2009, pp. 123–128.

[24] M.-Y. Cheng, C.-M. Tsao, Y.-Z. Lai, and Y.-J. Yang, "The development of a highly twistable tactile sensing array with stretchable helical electrodes," *Sensors Actuat., A*, vol. 166, no. 2, pp. 226–233, 2009.

[25] Y.-N. Cheung, Y. Zhu, C.-H. Cheng, and W. W.-F. L. C. Chao, "A novel fluidic strain sensor for large strain measurement," *Sensors Actuat., A*, vol. 147, no. 2, pp. 401–408, 2008.

[26] S. Wakimoto, K. Suzumori, and T. Kanda, "Development of intelligent McKibben actuator," in *Proc. IEEE/RSJ Int. Conf. Intell. Robot. Syst.*, Aug. 2005, pp. 487–492.

[27] S. Kuriyama, M. Ding, Y. Kurita, T. Ogasawara, and J. Ueda, "Flexible sensor for McKibben pneumatic actuator," in *Proc. IEEE Sensors Conf.*, Christchurch, New Zealand, Jan. 2009, pp. 520–525.
[28] S. Kuriyama, M. Ding, Y. Kurita, J. Ueda, and T. Ogasawara, "Flexible sensor for McKibben pneumatic artificial muscle actuator," *In. J. Autom. Tech.*, vol. 3, no. 6, pp. 731–740, 2009.
[29] M. D. Dickey, R. C. Chiechi, R. J. Larsen, E. A. Weiss, D. A. Weitz, and G. M. Whitesides, "Eutectic gallium-indium (EGaIn): A liquid metal alloy for the formation of stable structures in microchannels at room temperature," *Adv. Funct. Mater.*, vol. 18, no. 7, pp. 1097–1104, 2008.
[30] Y.-L. Park, B. Chen, D. Young, L. Stirling, R. J. Wood, E. Goldfield, and R. Nagpal, "Bio-inspired active soft orthotic device for ankle foot pathologies," in *Proc. IEEE/RSJ Int. Conf. Intell. Robot. Syst.*, San Francisco, CA, Sep. 2011, pp. 4488–4495.
[31] C. Majidi, R. Kramer, and R. J. Wood, "Non-differential elastomer curvature sensors for softer-than-skin electronics," *J. Smart Mater. Struct.*, vol. 20, no. 10, pp. 105017-1–105017-7, 2011.
[32] J. Paik, R. Kramer, and R. J. Wood, "Stretchable circuits and sensors for robotic origami," in *Proc. IEEE/RSJ Int. Conf. Intell. Robot. Syst.*, San Francisco, CA, Sep. 2011, pp. 414–420.
[33] R. Kramer, C. Majidi, and R. J. Wood, "Wearable tactile keypad with strethcable artificial skin," in *Proc. IEEE Int. Conf. Robot. Autom.*, Shanghai, China, May 2011, pp. 1103–1107.
[34] Y.-L. Park, C. Majidi, R. Kramer, P. Bérard, and R. J. Wood, "Hyperelastic pressure sensing with a liquid-embedded elastomer," *J. Micromech. Microeng.*, vol. 20, no. 12, p. 125029, 2010.
[35] J. Engel, J. Chen, Z. Fan, and C. Liu, "Polymer micromachined multimodal tactile sensors," *Sensors Actuat., A*, vol. 117, no. 1, pp. 50–61, 2005.
[36] Y. Tada, K. Hosoda, Y. Yamasaki, and M. Asada, "Sensing ability of anthropomorphic fingertip with multi-modal sensors," in *Proc. IEEE/RSJ Int. Conf. Intell. Robot. Syst.*, Las Vegas, NV, Oct. 2003, pp. 31–35.
[37] R. J. Whitney, "Measurement of changes in human limb volume by means of a mercury-in-rubber strain gauge," *J. Physiol.*, vol. 109 (supple), pp. 5P–6P, 1949.
[38] R. J. Whitney, "The measurement of volume changes in human limbs," *J. Physiol.*, vol. 121, no. 1, pp. 1–27, 1953.
[39] H. Tada, P. C. Paris, and G. R. Irwin, *The Stress Analysis of Cracks Handbook*, 3rd ed. New York: ASME, 2000.
[40] T. L. Anderson, *Fracture Mechanics: Fundamentals and Applications*, 3rd ed. New York: Taylor & Francis, 2005.
[41] A. F. Fernandez, F. Berghmans, B. Brichard, P. Mégret, M. Decréton, M. Blondel, and A. Delchambre, "Multi-component force sensor based on multiplexed fibre Bragg grating strain sensors," *Meas. Sci. Technol.*, vol. 12, no. 7, p. 810, 2001.
[42] P. Valdastri, S. Roccella, L. Beccai, E. Cattin, A. Menciassi, M. C. Carrozza, and P. Dario, "Characterization of a novel hybrid silicon three-axial force sensor," *Sensors Actuat. A*, vols. 123–124, no. 23, pp. 249–257, 2005.
[43] H. M. Herr and R. D. Kornbluh, "New horizons for orthotic and prosthetic technology: Artificial muscle for ambulation," in *Proc. SPIE, Smart Struct. Mater.: Electroact. Polym. Actuat. Devices*, Mar. 2004, pp. 1–9.
[44] L. Stirling, C. Yu, J. Miller, R. J. Wood, E. Goldfield, and R. Nagpal, "Applicability of shape memory alloy wire for an active, soft orthotic," *J. Mater. Eng. Perform.*, vol. 20, nos. 4–5, pp. 658–662, 2011.
[45] D. Shin, I. Sardellitti, Y.-L. Park, O. Khatib, and M. Cutkosky, "Design and control of a bio-inspired human-friendly robot," *Int. J. Robot. Res.*, vol. 29, no. 5, pp. 571–584, 2010.
[46] D. S. Kim, H. U. Lee, N. H. Kim, K.-H. Lee, D.-W. Cho, and T. H. Kwon, "Fabrication of microchannel containing nanopillar arrays using micromachined AAO (anodic aluminum oxide) mold," *Microelectron. Eng.*, vol. 84, nos. 5–8, pp. 1532–1535, 2007.
[47] D. C. Duffy, J. C. McDonald, O. J. A. Schueller, and G. M. Whitsides, "Rapid prototyping of microfluidic systems in poly (dimethylsiloxane)," *Anal. Chem.*, vol. 70, no. 23, pp. 4974–4984, 1998.
[48] Y. Xia and G. M. Whitsides, "Soft lithography," *Annu. Rev. Mater. Sci.*, vol. 28, pp. 153–184, Aug. 1998.
[49] R. K. Kramer, C. Majidi, R. Sahai, and R. J. Wood, "Soft curvature sensors for joint angle proprioception," in *Proc. IEEE/RSJ Int. Conf. Intell. Robot. Syst.*, San Francisco, CA, Sep. 2011, pp. 1919–1926.

Yong-Lae Park (M'10) received the M.S. and Ph.D. degrees in mechanical engineering from Stanford University, Stanford, CA, in 2005 and 2010, respectively.

He is currently a Technology Development Fellow with the Wyss Institute for Biologically Inspired Engineering, Harvard University, Boston, MA. His current research interests include fiber optic force and tactile sensing, design of soft wearable robots for human rehabilitation and artificial skin with embedded soft sensors and actuators, and development of novel manufacturing processes for microrobots and 3-D smart-robot-structures.

Bor-Rong Chen (M'10) received the Ph.D. degree in computer science from Harvard University, Boston, MA.

He was a Post-Doctoral Fellow with the Self-organizing Systems Research Group and the Wyss Institute for Biologically Inspired Engineering, Harvard University. He is currently the Chief Technology Officer with Biosensics LLC, Cambridge, MA. His current research interests include wearable sensors, low power embedded systems, and wireless networks.

Robert J. Wood (M'01) received the M.S. and Ph.D. degrees from the Department of Electrical Engineering and Computer Sciences, University of California, Berkeley, in 2001 and 2004, respectively.

He is currently an Associate Professor with the School of Engineering and Applied Sciences and the Wyss Institute for Biologically Inspired Engineering, Harvard University, Boston, MA. His current research interests include microrobotics and bioinspired robotics.